Molecular and Cellular Neuroscience 70 (2016) 30–41

Contents lists available at ScienceDirect

Molecular and Cellular Neuroscience

journal homepage: www.elsevier.com/locate/ymcne

Central and peripheral defects in motor units of the diaphragm of spinal muscular atrophy mice

Anuja Neve [a,b], Judith Trüb [a], Smita Saxena [a], Daniel Schümperli [a,*]

[a] Institute of Cell Biology, University of Bern, 3012 Bern, Switzerland
[b] Graduate School for Cellular and Biomedical Sciences, University of Bern, 3012 Bern, Switzerland

ARTICLE INFO

Article history:
Received 3 July 2015
Revised 30 October 2015
Accepted 23 November 2015
Available online 24 November 2015

Keywords:
Diaphragm
Perisynaptic Schwann cell
Proteomics
Motoneuron
Neuromuscular junction
Spinal muscular atrophy

ABSTRACT

Spinal muscular atrophy (SMA) is characterized by motoneuron loss and muscle weakness. However, the structural and functional deficits that lead to the impairment of the neuromuscular system remain poorly defined. By electron microscopy, we previously found that neuromuscular junctions (NMJs) and muscle fibres of the diaphragm are among the earliest affected structures in the severe mouse SMA model. Because of certain anatomical features, i.e. its thinness and its innervation from the cervical segments of the spinal cord, the diaphragm is particularly suitable to characterize both central and peripheral events. Here we show by immunohistochemistry that, at postnatal day 3, the cervical motoneurons of SMA mice receive less stimulatory synaptic inputs. Moreover, their mitochondria become less elongated which might represent an early stage of degeneration. The NMJs of the diaphragm of SMA mice show a loss of synaptic vesicles and active zones. Moreover, the partly innervated endplates lack S100 positive perisynaptic Schwann cells (PSCs). We also demonstrate the feasibility of comparing the proteomic composition between diaphragm regions enriched and poor in NMJs. By this approach we have identified two proteins that are significantly upregulated only in the NMJ-specific regions of SMA mice. These are apoptosis inducing factor 1 (AIFM1), a mitochondrial flavoprotein that initiates apoptosis in a caspase-independent pathway, and four and a half Lim domain protein 1 (FHL1), a regulator of skeletal muscle mass that has been implicated in several myopathies.

1. Introduction

Spinal muscular atrophy (SMA) is an autosomal recessive disorder characterized by a degeneration of the alpha motoneurons in the ventral horn of the spinal cord. In the human genome, the SMA determining Survival Motor Neuron (*SMN*) gene exists in two forms, *SMN1* and its paralogue *SMN2* (Schmutz et al., 2004). Although these copies are nearly identical (Lefebvre et al., 1995), a critical difference at position +6 of exon 7 (Lorson et al., 1999; Monani et al., 1999) results in alternatively spliced mRNA transcripts from the *SMN2* gene. These transcripts lack exon 7 and encode a highly unstable, truncated protein (Cartegni et al., 2006; Cartegni and Krainer, 2002; Kashima and Manley, 2003; Lorson et al., 1999). Nevertheless, the *SMN2* gene also produces low levels of functional, full-length SMN mRNA and protein (Lorson and Androphy, 2000). In 95% of human SMA cases, the *SMN1* gene is absent (Burghes, 1997; Lefebvre et al., 1995) while in the remaining 5%, it carries small deletions or mutations (Alías et al., 2009; Rodrigues et al., 1995). Hence, the primary cause of SMA is a low level of functional SMN protein produced from the remaining *SMN2* gene copy/copies.

The classical features of SMA include loss of motoneurons (MNs), muscle atrophy and profound muscle weakness. In human SMA patients, the proximal muscles have been found to be more affected than distal ones with intercostals and paraspinal muscles being more affected than the diaphragm, which is relatively spared (Crawford, 2003). However, studies on mouse models have indicated that the diaphragm is strongly affected (Kariya et al., 2008; Michaud et al., 2010; Voigt et al., 2010), and a more focused analysis revealed similar changes in the diaphragm of 6 month old human SMA type I patients (Kariya et al., 2008).

For the severe mouse SMA model (Monani et al., 2000), we have previously found by transmission electron microscopy that the diaphragm is one of the earliest affected muscles (Voigt et al., 2010, 2014). At postnatal day 3 (PND3), this muscle shows a spectrum of neuromuscular

Abbreviations: AIFM1, apoptosis inducing factor 1; ALS, Amyotropic Lateral Sclerosis; BTX-Rho, rhodamine-conjugated α-bungarotoxin; ChAT, choline acetyltransferase; FHL1, four and half lim domain 1; GlyT2, glycine transporter 2; Hsp60, heat shock protein 60; IHC, immunohistochemistry; MN, motoneuron; NDUFA9, nicotinamide adenine dinucleotide dehydrogenase (ubiquinone) 1, alpha subcomplex, 9; NMJ, neuromuscular junction; PANTHER, Protein Analysis Through Evolutionary Relationships; PBS, phosphate buffered saline; PFA, paraformaldehyde; PMSS, Protein Match Score Summation; PND, postnatal day; PSC, perisynaptic Schwann cell; SMA, spinal muscular atrophy; SMN, Survival Motor Neuron; SYP, synaptophysin; VAChT, vesicular acetylcholine transporter; VGAT, vesicular GABA transporter; VGLUT1, vesicular glutamate transporter 1; wt, wild-type.

* Corresponding author at: Institute of Cell Biology, University of Bern, Baltzerstrasse 4, 3012 Bern, Switzerland.
E-mail address: daniel.schuemperli@izb.unibe.ch (D. Schümperli).

http://dx.doi.org/10.1016/j.mcn.2015.11.007

junction (NMJ) alterations ranging from normal appearance to severely affected NMJs. The most strongly affected NMJs were characterized by massive mitochondrial swellings in the axon terminals and muscle fibres. Furthermore, the perisynaptic Schwann cells (PSCs) which are the glial components of the NMJ and play an important role in the structure, function and maintenance of the NMJ (Auld and Robitaille, 2003) exhibited electron-translucent vacuole-like profiles and a darkly contrasted cytoplasm (Voigt et al., 2010).

Less severe changes were observed in the intercostal muscles while calf muscles, which were still relatively immature, showed no ultrastructural changes. This correlation of pathology with the developmental stage of these three muscles suggested that, for SMA-related changes to occur, the muscles have to reach a certain critical stage of developmental maturity (Voigt et al., 2014).

Here, our goal has been to shed more light on the relatively poorly understood pathogenic mechanisms that lead to these muscle defects. The earliest affected muscle in the severe mouse SMA model, the diaphragm, is very thin, and its NMJs are aligned in a band along the phrenic nerve. These properties make it uniquely suitable for whole mount immunohistochemistry and biochemical analyses of muscle areas enriched in NMJs. Moreover, as the MNs innervating the diaphragm are located in the cervical region of the spinal cord and represent a large fraction of the MNs in this region, we were able to study not only the SMA-related synaptic defects occurring in the diaphragm but also the corresponding MN circuitry.

Our results reveal several alterations that are likely to impair the proper function of the diaphragm's motor units. For the MN cell bodies in the spinal cord, an imbalance of synaptic inputs (reduced excitatory and unchanged numbers of inhibitory synapses) and abnormal appearing mitochondria represent early defects that occur prior to MN death. Peripheral NMJs show a reduction of synaptic vesicles and active zones as well as PSCs with weak S100 immunoreactivity. Moreover, a proteomic analysis reveals changes that can be interpreted as compensatory reactions to these deficits and an onset of cell death mechanisms. Together, these events may synergistically contribute to the dysfunction of this important respiratory muscle.

2. Materials and methods

2.1. Mice

Smn$^{+/-}$; *SMN2*$^{+/+}$ mice (Jackson labs strain name: FVB.Cg-Tg (SMN2) 89 Ahmb Smn1^{tm1Msd}/J, stock number: 005024) were maintained as heterozygote breeding pairs under standard IVC conditions in the animal facility at the Insel hospital in Berne, Switzerland, complying with legal requirements for animal husbandry. The mean survival of the SMA-affected offspring (*Smn*$^{-/-}$; *SMN2*$^{+/+}$), under our breeding conditions is 6.5 days. In some experiments we also used mice of the same strain containing multiple copies (~5) of the U7-ESE-B gene that corrects *SMN2* splicing and ameliorates the SMA phenotype (Meyer et al., 2009).

2.2. Immunohistochemistry

Immunohistochemistry (IHC) experiments of whole mount diaphragms were performed as previously described (Voigt et al., 2014). For triple labelling experiments, mice were perfused with 4% PFA. In order to facilitate better penetration of the antibodies, the samples were incubated with the primary antibodies sequentially. The muscles were flat mounted in Vectashield (Reacto labs).

Spinal cords were obtained as follows: animals at PND3 were anaesthetized on ice for 8 min for wt or 6 min for diseased mice (because of their smaller body size). The animals were perfused with phosphate-buffered saline (PBS), and the spinal cords were fixed in 10 ml of 4% paraformaldehyde (PFA) overnight at 4 °C followed by placing them in 30% sucrose (w/v). The cervical region was excised and embedded in cryomolds using tissue tek optimal cutting temperature formulation (Sakura Finetec, USA) and stored at −20 °C. The embedded spinal cord segments were sectioned at 20 μm thickness with a microtome. Each section was 200 μm apart from the next, and 10 such sections were collected on a Superfrost ultra plus slide (GroggChemie, 6310650). Every 6th slide was used for analysis. The slides were completely air-dried for 4–5 h at room temperature, and sections were fixed in 4% PFA for 10 min. After washes in PBS, the sections were blocked in 3% BSA, 0.5% Triton in PBS for 1 h at 4 °C. For mitochondrial stainings, after PFA fixation, antigen retrieval was performed according to standard procedures (citrate/heat method). The incubations with primary antibodies were performed overnight (or for three days for the mitochondrial analyses) at 4 °C, followed by 3 washes in PBS. Secondary antibodies were incubated for 3 h at room temperature. After these incubations and 3 additional washes, the slides were air dried and mounted in Vectashield. The primary and secondary antibodies and direct probes used for these experiments are listed in the Supplementary Table S1.

2.3. Imaging

The imaging was done with Leica SP5 or SP8 confocal microscopes while using a 63× oil objective. The same settings were used for wt and disease samples. Z stacks were made at 0.5 μm step size, and maximum intensity projections were made with Image J software. The overlay between the two channels was assessed with the help of Adobe Photoshop. For S100 IHC, after classifying *en face* endplates, intensity measurements were made using Image J software. For bassoon IHC, measurements of bassoon puncta were done with Imaris software. For each genotype, a minimum of 50 endplates were selected at random from the top, middle and bottom regions of the diaphragm of two animals. For quantification of motoneuron synapses, the specific synapses around a minimum of 80 motoneurons from three animals per genotype were counted. Synapses located within a perimeter of 100 μm around a motoneuron were quantified with the Imaris software. Mitochondrial imaging was done with a Leica SP8 confocal microscope using a 100× oil objective. Sphericity and area were measured using Imaris software. The significance of differences was assessed by using Mann–Whitney test, two tailed (GraphPad Prism 5).

2.4. Global protein analysis

To identify new proteins at the NMJs that could cause or contribute to SMA pathology, mass spectrometry analysis was carried out. Samples used were snap frozen diaphragm muscles isolated at PND3 from three PBS-perfused mice of each genotype, i.e. wt, SMA disease and SMA mice containing multiple copies of the U7-ESE-B therapeutic construct that corrects the SMA phenotype (Meyer et al., 2009). To separate the synaptic component of the muscle from its extra-synaptic counterpart, the muscles were stained with tetramethylrhodamine-conjugated α-bungarotoxin (Molecular Probes, T1175) diluted 1:500 in PBS containing 1× Protease Inhibitor cocktail. Manual dissection was performed under a fluorescent dissecting microscope (Olympus, SZX10 at 2× magnification). Protein extractions were performed using RIPA buffer (50 mM Tris pH 8.0, 150 mM NaCl, 1% Nonidet P40, 0.1% SDS, 0.5% sodium deoxycholate), and samples were subjected to SDS-PAGE. After Coomassie staining and destaining, the gel bands were cut with a surgical blade (Grogg, number 22) into small cubes (~1 mm^3), and not more than six such cubes were placed in an Eppendorf tube containing 20% ethanol. If the samples were not submitted to the proteomics core facility on the same day, they were stored at 4 °C overnight.

2.5. Immunoblotting

To validate the candidates, Western blots were performed from the proteins extracted from wt and SMA mice. Sample preparation and

protein extraction remained exactly as explained above. The protein samples were run on a 12% SDS polyacrylamide gel. The proteins were transferred from the gel to a polyvinylidenefluoride (PVDF) membrane (Roche) for 1.5 h at 135 mA by using a semi-dry blotting system (Witec AG). The membranes were blocked for 1 h in a blocking buffer containing 5% milk and then incubated overnight in primary antibodies diluted in 5% milk PBS-Tween (PBS-T) at 4 °C. After three washes with PBS-T, the secondary antibodies diluted in 5% milk PBS-T were incubated for 1 h at room temperature. The primary and secondary antibodies used for these experiments are listed in the Supplementary Table S1. Horseradish peroxidase activity was detected by enhanced chemiluminescence (Amersham ECL prime Western blotting detection reagent kit, GE healthcare life sciences, RPN 2232) according to the manufacturer's instructions. The signal intensity was quantified using the Advanced Imager Data Analyser software (AIDA, version 3.11.002), and the results were normalized to those obtained for TFIIH.

3. Results

3.1. Motoneurons of the cervical segments of severe SMA mice show an imbalance of synaptic inputs and mitochondrial abnormalities

As we had previously shown that, on post-natal day 3 (PND3), the diaphragm shows the strongest alterations in the severe SMA model (Voigt et al., 2010, 2014), we now focused on identifying disease-relevant alterations within the motoneurons that innervate this important respiratory muscle. Thus, we specifically examined the cervical segments of the spinal cord from which the diaphragm is innervated. Neural circuits within the spinal cord play an important role in controlling motor behaviour. In particular, MNs are known to receive multiple inputs from primary Ia afferent fibres, Renshaw cells, Ia inhibitory interneurons, serotoninergic axons and descending pathways (Cope, 2001). A balance between the excitatory and inhibitory inputs is necessary for proper tonic firing of MNs. Disruptions in the spinal circuitry have been implicated in ALS (Chang and Martin, 2009; Jiang et al., 2009; Schütz, 2005) and a few studies have shown a reduction in stimulatory/proprioceptive inputs in the milder SMA Δ7 model (Ling et al., 2010; Mentis et al., 2011). We examined the excitatory glutamatergic inputs by using anti-vesicular glutamate transporter 1 (VGLUT1) (Fig. 1A) and the inhibitory glycinergic synapses using anti-gephyrin (specific for the post-synaptic part of the inhibitory synapses) (Fig. 1B) and anti-glycine transporter 2 (GlyT2) (Fig. 1C). Cholinergic MNs were identified using anti-choline acetyl transferase (ChAT) (Fig. 1A–C). Upon statistical analysis, a signification reduction (~50%) in the average number of VGLUT1 positive, excitatory synapses onto MNs was observed in the SMA disease mice on PND3 in comparison to the wt littermates (Fig. 1D). With respect to the inhibitory synapses, no significant difference in the average number of gephyrin or GlyT2 synapses around the MNs was seen between wt and disease mice (Fig. 1E and F, respectively).

MNs have a high requirement for Ca^{2+} buffering and ATP and are therefore heavily dependent on proper mitochondrial function (Baker et al., 2011). Thus, the MN survival and function strongly depends on the integrity and functionality of mitochondria. Furthermore, mitochondria often undergo changes in morphology in response to environmental and cellular stressors (Barbour and Turner, 2014). Therefore, we wanted to examine if the gross morphology of the mitochondria in cervical MNs is altered in SMA mice. We used an antibody against heat shock protein 60 (Hsp60) as a marker for the mitochondrial matrix and anti-vesicular acetylcholine transporter (VAChT) to identify cholinergic neurons in cervical spinal cord sections of wt and SMA disease animals (Supplementary Fig. S1A). These analyses revealed that, in comparison to wt mice, SMA mice have mitochondria that appear more condensed and round as opposed to the normal elongated shape. This was further supported by quantifications of the sphericity and area of each mitochondrion, in the sense that mitochondria of SMA disease mice were significantly more spherical (i.e. rounder) (Supplementary Fig. S1B) and displayed a smaller area (Supplementary Fig. S1C) than those of wt mice. Such a transition in mitochondrial morphology is reminiscent of that observed in COS-7 cells which had been induced to enter apoptosis experimentally (Frank et al., 2001).

Taken together, these results reveal molecular/organellar changes in the cervical MNs that precede gross morphological alterations or MN loss. In particular, the imbalance between stimulatory and inhibitory synaptic inputs is likely to affect MN function.

3.2. Axon terminals in the diaphragm muscle of SMA mice show reduced synaptic vesicle coverage and active zone density

We have previously shown that a subset of the NMJs of the diaphragm of SMA mice show strong morphological changes at the ultrastructure level on PND3 (Voigt et al., 2010) (see Introduction). Moreover, 26% of the NMJs (presumably the same ones that show the ultrastructural changes) were found to be partly innervated compared to only 11% in wt animals (Voigt et al., 2014). To understand how this affects the organization of the pre-synaptic components, we investigated the total endplate area covered by synaptic vesicles as well as the active zone density. Synaptophysin (Fig. 2A) and bassoon (Fig. 2B and C) were used as respective markers for these two parameters, and post-synaptic acetylcholine receptors at the NMJs were labelled with rhodamine conjugated α-bungarotoxin (BTX-Rho). At PND3, there was a significant reduction in the area occupied by the synaptic vesicles in SMA animals in comparison to the wt littermates (Fig. 2D). In fact, the total surface area covered by the synaptic vesicles was ~20% smaller in SMA mice. Similarly, we also observed that the active zones were less densely distributed in SMA mice compared to wt mice (Fig. 2B). Quantitatively, both the active zone area (Fig. 2E) and density (Fig. 2F) were significantly reduced. Together with the previously observed ultrastructural changes and the partial innervation, our data indicates that a substantial subset of the diaphragm NMJs in PND3 SMA mice are strongly impaired so that the changes are significant at the whole population level.

3.3. PSCs capping the partly innervated NMJs of SMA mice show reduced S100 immunoreactivity

Our previously published electron microscopy analyses of the diaphragm NMJs at PND3 had revealed electron translucent vacuole-like profiles in the cytoplasm of the PSCs in SMA mice (Voigt et al., 2010). Here, we wanted to investigate this phenomenon with an established Schwann cell marker. For this purpose, we performed a triple labelling of the PND3 diaphragm NMJs. The motor endplates were stained with α-bungarotoxin (Fig. 3A and B, blue), and nerve terminals were labelled with neurofilament antibody (green). Anti-S100 antibody (red) was used to visualize PSCs. The endplates were classified as fully (white arrows in Fig. 3A and B) or partly innervated (yellow arrows) based on the arborization of the nerve terminal. The proportions of partly innervated NMJs were similar to the previously reported ones (Voigt et al., 2014) (i.e. 26% and 11% for SMA and wt animals, respectively). Separate visualizations of the three analysed markers are shown for selected NMJs in Fig. 3C–F. Note that the partly innervated endplate of an SMA mouse shows no detectable S100 staining (Fig. 3F), whereas fully innervated endplates of wt and SMA mice as well as a partly innervated one from a wt mouse are positive for S100 (Fig. 3C–E). Importantly, the intensity of S100 staining is significantly reduced for the entire population of partly innervated endplates in SMA mice compared to wt littermates (Fig. 3H). In contrast, no significant changes in the S100 intensity were seen between the fully innervated endplates of SMA and wt mice (Fig. 3G). The implications of this reduced S100 staining will be elaborated in the Discussion section.

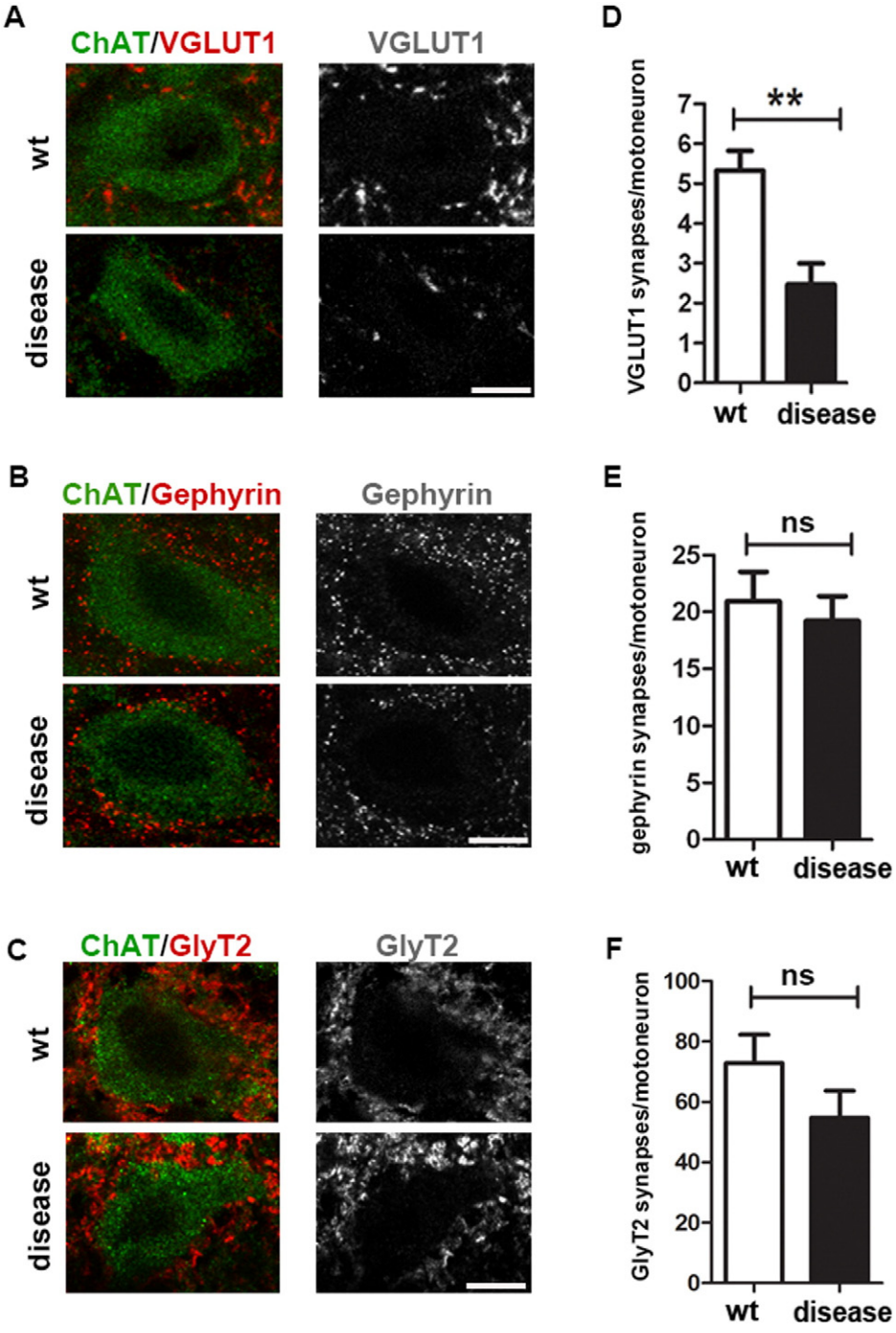

Fig. 1. Imbalance of synaptic inputs onto cervical motoneurons of SMA mice. (A) Cervical spinal cord segments were immunolabelled with anti-ChAT as a marker to identify cholinergic neurons (green) and anti-VGLUT1 (red) to study excitatory glutamatergic synapses in wt and disease mice. Inhibitory glycinergic synapses were examined using (B) anti-gephyrin (red) and (C) anti-GlyT2 (red). MNs were identified as in A. (D) A significant reduction in the average number of excitatory synapses was seen in the MNs of disease mice in comparison to the wt littermates. (E, F) With respect to the inhibitory synapses, no significant difference was observed. Perimeter around MNs kept at 100 μm (n = at least 80 MNs from 3 mice per genotype, Mann Whitney two-tailed test, **P = 0.005). Scale bars (A and B) 5 μm.

3.4. Global analysis of proteins from synaptic areas of SMA mouse diaphragm reveals extensive changes in mitochondrial proteins and additional regulatory molecules

To gain more insight into the molecular events occurring in our system, we tried to identify proteins that are specifically altered in their expression at the NMJs and might hence cause or contribute to SMA pathology. As the isolation of NMJs by laser capture microdissection was unlikely to yield proteins in sufficient quantity and quality for proteomic analysis (P. Odermatt and D.S., unpublished observation), we had to use a different approach. The fact that the diaphragm is very thin and that the NMJs are aligned in a narrow band along the phrenic nerve (Fig. 4A) allowed us to dissect regions highly enriched in NMJs manually under a fluorescent dissecting microscope after staining with BTX-Rho. To validate this type of synaptic enrichment, Western blots were probed with anti-synaptophysin antibody. This revealed that synaptophysin expression is almost exclusively detectable in the synaptic and not in the extra-synaptic fraction (Fig. 4B). Protein samples from

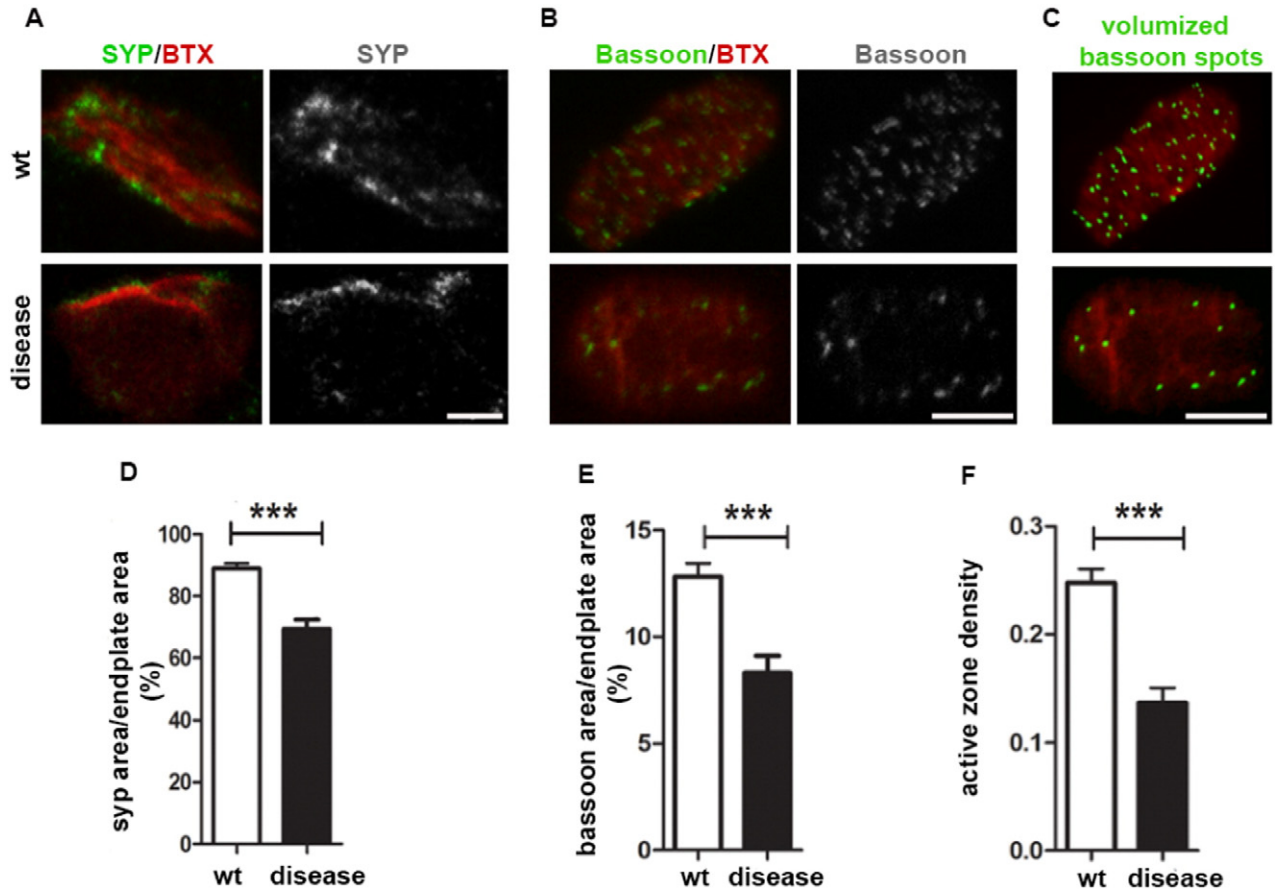

Fig. 2. Pre-synaptic defects in the diaphragm muscle of SMA mice at PND3. (A) NMJs of wt and SMA mice were labelled by immunofluorescence for synaptophysin (SYP, green) and endplates were labelled using bungarotoxin (BTX, red). (B) Active zones were identified by immunostaining for bassoon (green), and endplates were labelled as in A. Wt NMJs had compact, densely distributed active zones as opposed to the disease NMJs, in which the active zones were sparse. (C) The bassoon puncta are represented as volumized spots using the Imaris software. (D) A significant reduction in the area occupied by the synaptic vesicles over the endplates was seen in the SMA mice (n = at least 50 NMJs per genotype, 2 mice each, Mann Whitney two-tailed test, ***$P < 0.0001$). (E) The area of the bassoon positive spots was calculated and normalized to the total number of endplates. Significant reduction was seen in the SMA mice (n = at least 50 NMJs per genotype, 2 mice each, Mann Whitney two-tailed test, ***$P = 0.0002$). (F) The active zone density was also significantly reduced in SMA mice (n = at least 50 NMJs per genotype, 2 mice each, Mann Whitney two-tailed test, ***$P < 0.0001$). Scale bars: (A) 3 μm, (B and C) 5 μm.

the synaptic and extra-synaptic regions of the diaphragm of three SMA disease, wt and SMA/U7 mice were then digested into peptides and analysed by nano LC–MS/MS with a LC gradient and searched with Easyprot and or MaxQuant/Andromeda against a non-redundant database. After elimination of likely contaminants (human keratins, bovine serum components) and proteins detected infrequently and not in all three genotypes of the analysed diaphragm section, we obtained data for 416 and 450 proteins from the synaptic and extra-synaptic fractions, respectively (Table 1). The original data from this proteomic analysis are available as a Supplementary File S2 (Excel format) at the journal website..

To evaluate these candidate proteins, the fold change in Protein Match Score Summation (PMSS; an indicator of protein abundance) was calculated, normalized to the PMSS value of actin in the same sample, and groups of proteins showing a greater than 2-fold or a 1.5- to 2-fold increase or decrease between the corresponding SMA and wt samples were formed. The numbers of proteins falling into these different groups are listed in Table 1. Notably, despite the fact that 314 proteins were present in both the synaptic and extra-synaptic samples of wt animals, the groups of up- and down-regulated proteins from the two diaphragm regions contained only 42 identical proteins of which 10 and 11 were similarly up- or down-regulated in both regions (resulting in 21 convergent changes altogether). The other 21 proteins showed an up-regulation in one and a down-regulation in the other sample. Moreover, synaptophysin-like protein 2 (SYPL2) was the protein most highly enriched in the synaptic fraction of wt mice compared to the corresponding extra-synaptic sample (3.9-fold). Even though we had detected synaptophysin by Western blot (Fig. 4B), it was not present in our lists of proteins identified by MS. A list of all proteins enriched at least 1.5 fold in the synaptic sample is shown in Supplementary Table S2.

The average PMSS values (relative to actin) across the entire protein libraries showed only very minor changes between the three mouse genotypes (Fig. 4C; where the actin-normalized wt value is always set as 1). In contrast, the average values of the different selected groups showed the expected greater than 2- or 1.5-fold increases and decreases in the SMA samples. Interestingly, for most of the groups, the samples of the SMA/U7 mice had PMSS values between those of the wt and SMA genotypes, indicating a partial rescue of the changes.

The molecular functions of the 170 proteins that had shown more than 1.5-fold changes (up or down) in the synaptic samples of SMA animals compared to wt were then analysed with the PANTHER software (Protein Analysis Through Evolutionary Relationships). The most important group of altered proteins (43.2%) are catalytic (mostly mitochondrial) proteins playing an important role in the respiratory electron transport chain, or in mitochondrial transport, proteolysis, oxidative phosphorylation, protein acetylation or apoptosis (Table 2). This is particularly interesting, considering that we had observed massive mitochondrial degenerations in axon terminals and sub-synaptic muscle fibres in our previous electron microscopic analyses (Voigt et al., 2010,

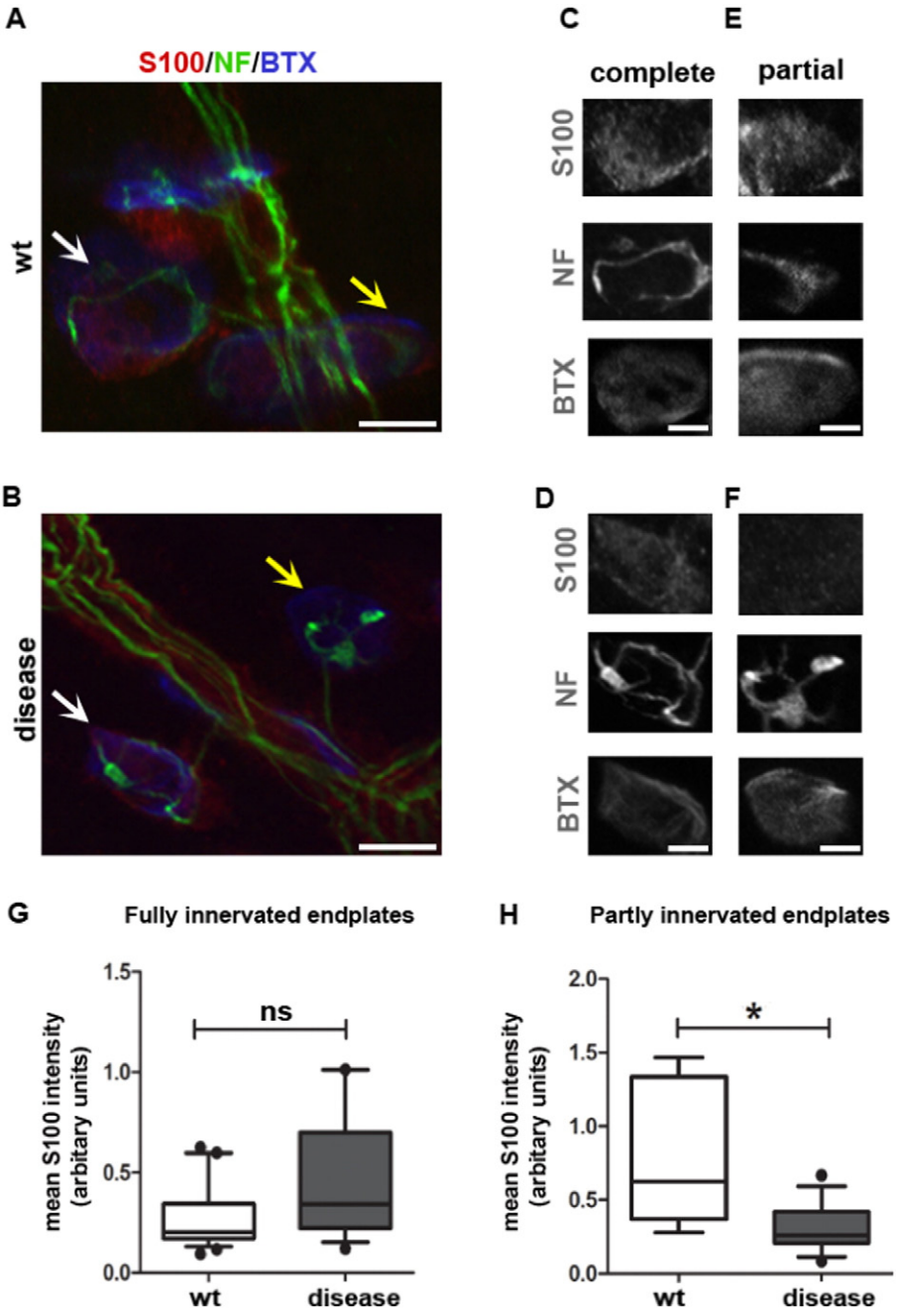

Fig. 3. Reduced S100 intensity of perisynaptic Schwann cells (PSCs) capping the partly innervated NMJs of SMA mice. (A, B) Confocal micrographs of diaphragms immunohistochemically labelled with anti-neurofilament antibody to visualize pre-synaptic nerve terminals (green), anti-S100 to visualize PSCs (red) and Alexa fluor647-conjugated-alpha bungarotoxin (blue) to label post-synaptic endplates in wt and SMA mice, respectively. The endplates were classified as completely (white arrows) or partly innervated (yellow arrows) based on the occupancy of the nerve terminal. (C, D, E) At completely innervated endplates of wt and SMA mice and also at a partly innervated endplate of a wt mouse, a S100 positive PSC can be seen capping the NMJs. (F) However, a partly innervated end plate of an SMA mouse shows no detectable S100 staining of PSC. (G) Quantification of the mean S100 intensity reveals no significant difference for PSCs capping fully innervated endplates in wt and SMA mice (n = at least 50 NMJs per genotype, 2 mice each, Mann Whitney two-tailed test, P = 0.05). (H) However, there is a significant reduction in the mean S100 intensity for PSCs capping party innervated endplates in SMA mice in comparison to wt littermates (n = at least 50 NMJs per genotype, 2 mice each, Mann Whitney two-tailed test, *P = 0.01). Scale bars (A and B) 10 μm, (C, E, D and F) 5 μm.

2014). When only the up-regulated proteins were considered, this functional group even amounted to 56.8%. The other important subsets of proteins have binding activity (mostly transcription and translation factors or cytoskeletal components) and structural molecule activity (Table 2). The sample is very significantly enriched in the following PANTHER GO-Slim biological processes: generation of precursor metabolites and energy ($P = 1.79 \times 10^{-12}$), oxidative phosphorylation ($P = 4.33 \times 10^{-12}$) and respiratory electron transport chain ($P = 9.04 \times 10^{-9}$).

For an initial validation of these proteomics results, we selected two mitochondrial proteins, i.e. apoptosis inducing factor 1 (AIFM1) and nicotinamide adenine dinucleotide dehydrogenase (ubiquinone) 1 alpha subcomplex, 9 (NDUFA9), and one regulatory protein implicated in several myopathies, four and half lim domain 1. Besides their biological interest, these proteins had shown a range of up-regulation in the synaptic region of SMA animals compared to the controls (Fig. 5A). Moreover, all of them showed only minimal changes in the extrasynaptic part (Fig. 5A), suggesting that their up-regulation was specific

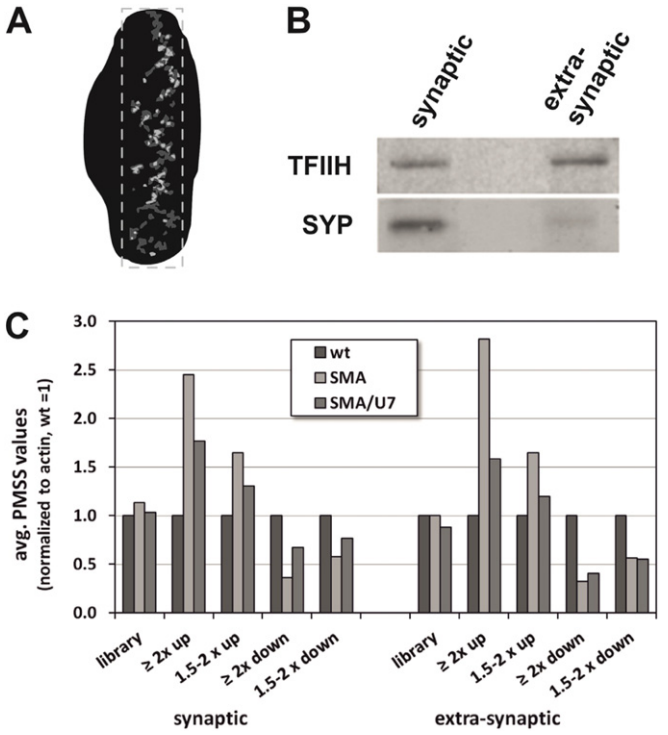

Fig. 4. Identification of alterations in the synaptic proteome of the diaphragm muscle. (A) Schematic representation of the diaphragm muscle immunolabelled using BTX-Rho. Due to pre-patterning, the NMJs are aligned as a central band along the muscle. The dashed line approximates how the synaptic and extra-synaptic regions of the muscle were separated under a fluorescent dissecting microscope. (B) Western blots of the proteins extracted from synaptic and extra-synaptic regions of three SMA carrier mice ($Smn^{+/-}$; $SMN2^{+/+}$) revealed that synaptophysin (SYP) was specifically enriched in the synapse-specific region. TFIIH was used as a loading control. (C) Average PMSS values (a proxy for protein abundance in a proteomic sample) of complete synaptic and extra-synaptic protein libraries and of selected subgroups showing the indicated up- and down-regulations of PMSS values. Note that the increases or decreases caused by the SMA genotype are in most graphs partly compensated in SMA/U7 mice that contain the U7-ESE-B therapeutic construct which partly corrects the SMA phenotype (Meyer et al., 2009).

to the NMJ. These candidates were validated by Western blotting (Fig. 5B), and statistical analyses revealed that indeed AIFM1 and FHL1 are significantly up-regulated (1.8- and 3-fold, respectively) in the synaptic regions of SMA mouse diaphragms (Fig. 5C). The third candidate, NDUFA9, also showed a higher level of expression in the SMA synapse-specific region, but this was not statistically significant (Fig. 5C). We also noticed that FHL1 appeared to be slightly reduced in the extra-synaptic samples. FHL1 and AIFM1 were additionally analysed by Western blotting in samples from the cervical region of the spinal cord (Supplementary Fig. S2). Both proteins could be detected, but neither of them showed any difference between WT and SMA mice. This underlines that the difference we have observed is specific for the NMJ-enriched part of the diaphragm.

Table 1
Summary of proteomic analysis.

Protein numbers:	Synaptic	Extra-synaptic	Overlap
≥2× up	53	35	2
≥2× down	30	52	4
1.5–2× up	59	47	2
1.5–2× down	28	45	4
Sum	170	179	21[b]
Total identified[a]	416	450	314

[a] After elimination of likely contaminants and proteins detected at low levels and not in all three samples.
[b] Only convergent changes considered.

4. Discussion

Even though SMA has been studied quite extensively, and motoneurons which innervate the skeletal muscles are obviously responsible for the most severe symptoms (Crawford, 2003), it is still not clear which processes are primarily responsible for the malfunctioning of the neuromuscular system. An initial idea that a particular fibre type could be preferentially susceptible to SMA (Murray et al., 2008) was recently challenged (Ling et al., 2012; Thomson et al., 2012). Even in the most severe mouse SMA models, it appears that motoneurons and NMJs are formed normally and that the SMA-dependent alterations are primarily of a degenerative nature (McGovern et al., 2008; Murray et al., 2008, 2010b; Voigt et al., 2010). Moreover, morphological defects in the periphery, in particular at the NMJs, have been found to precede any overt changes in motoneurons (Dachs et al., 2011; Murray et al., 2008, 2010b; Voigt et al., 2010).

To characterize processes involved in the emergence of SMA, we have analysed several aspects of the neuromuscular system specifically for the diaphragm of severe SMA mice at PND3. The choice of this particular system was governed by several considerations. First, the diaphragm is an important respiratory muscle that is also relevant for SMA, at least in severe mouse models (Michaud et al., 2010; Voigt et al., 2010, 2014). We also note that degenerative changes of the diaphragm have been described in 6 months old human SMA type I patients (Kariya et al., 2008). Additionally, the diaphragm is one of the earliest affected muscles in the severe SMA mouse model and shows a spectrum of NMJ abnormalities. Moreover, its thinness and the alignment of NMJs along a narrow band accompanying the phrenic nerve render the diaphragm particularly suited for the types of analyses performed here. Last but not least, the phrenic nerve originates in the central cervical segments of the spinal cord and thus represents a major fraction of the cervical motoneuron population. These features have enabled us to study both central and peripheral aspects of motor units affected in SMA by immuno-histochemical and proteomics techniques. To our knowledge, this is the first time that such a comprehensive analysis has been performed for this disease-relevant muscle. This approach opens the view on possible connections between pathological events occurring in the spinal cord and the corresponding muscle.

Our previous ultrastructural investigations (Voigt et al., 2010, 2014) had allowed us to distinguish three subpopulations of diaphragm NMJs with respect to SMA pathology. Besides normal looking NMJs, there were weakly and strongly affected ones. The more weakly affected NMJs showed small vacuole-like inclusions and a more darkly contrasted cytoplasm in PSCs but no obvious changes in the axon terminals and muscle fibres. In addition to these changes in PSCs, the more strongly affected NMJs also had massively swollen mitochondria in the axon terminals and the underlying muscle fibre areas. At PND3, these three NMJ phenotypes were present in roughly equal numbers. Moreover, we detected that 26% of the NMJs, presumably representing the more strongly affected group, showed a partial denervation (Voigt et al., 2014). This was accompanied by a significant increase in pre- and post-synaptic defects such as neurofilament accumulation, improper nerve terminal branching, and reduced acetylcholine receptor area.

The fact that the numbers and overall morphology of motoneuron cell bodies are normal at PND3 in the severe mouse SMA model (Monani et al., 2000) does not exclude that the motoneurons could be impaired. To analyse if this is the case, we have studied two important functional aspects, i.e. the balance of excitatory to inhibitory synaptic inputs and the morphology of mitochondria. A balance of synaptic inputs onto the motoneurons is crucial for their tonic firing and activity. Excitotoxicity caused by a gain of excitatory signalling has been implicated in the death of motoneurons in ALS (Chang and Martin, 2009; Jiang et al., 2009; Schütz, 2005). In this study, we observed no changes in the number of inhibitory GlyT2 synapses or in the post-synaptic part of inhibitory synapses by analysing gephyrin. However, we

Table 2
Molecular function analysis of proteins up- or down-regulated in diaphragm synaptic region of SMA compared to wt animals at PND3.

GO molecular function	Hits	% of hits	Comment
Catalytic activity (GO:0003824)	41	43.2	Metabolic (mostly mitochondrial)
Binding (GO:0005488)	23	24.2	Nucleic acid, protein (cytoskeleton)
Structural molecule activity (GO:0005198)	17	17.9	Cytoskeleton, ribosome
Enzyme regulator activity (GO:0030234)	5	5.3	Myosins
Receptor activity (GO:0004872)	4	4.2	
Transporter activity (GO:0005215)	3	3.2	
Antioxidant activity (GO:0016209)	2	2.1	
Total	95	100	

Analysis of the 170 proteins that showed at least a 1.5-fold up- or down-regulation in synaptic region. The analysis was performed online at http://www.pantherdb.org/(last accessed 30.06.2015). Note that not all proteins were identified by the software.

detected a drastic (~50%) reduction in the number of excitatory vesicular glutamate transporter 1 (VGLUT1) synapses in the cervical region of the spinal cord of the severe SMA mice (Fig. 1). Previous studies on lumbar spinal cord segments of Δ7 SMA mice have also demonstrated a reduction in VGLUT1 synapses (Ling et al., 2010; Mentis et al., 2011) as well as a reduced response to proprioceptive input signals (Mentis et al., 2011). Reduced VGLUT1 synapses were also seen in a mouse model with selective reduction of SMN in motoneurons (Park et al., 2010). Furthermore, a disruption of motor circuit activity due to defective synaptic inputs onto motoneurons has been shown in a *Drosophila* model of SMA (Imlach et al., 2012). Last but not least, there is also evidence for a degeneration of sensory axons in SMA type I patients (Anagnostou et al., 2005; Rudnik-Schöneborn et al., 2003), suggesting that the situation regarding stimulatory inputs may be similar as in mouse models. One reason for this phenomenon could be a retarded growth of sensory axon terminals (shorter neurites and smaller growth cones) as has been demonstrated in an in vitro study of isolated sensory neurons from E14 SMA severe embryos (Jablonka et al., 2006).

Regarding inhibitory synapses, we could only identify one previous study. In the already mentioned analysis of Δ7 SMA mice, Ling, Ko and coworkers also analysed vesicular GABA transporter (VGAT) synapses and found no significant changes (Ling et al., 2010). We have not analysed VGAT activity because of a report that such synapses may switch from excitatory to inhibitory activity in young mice (Ben-Ari

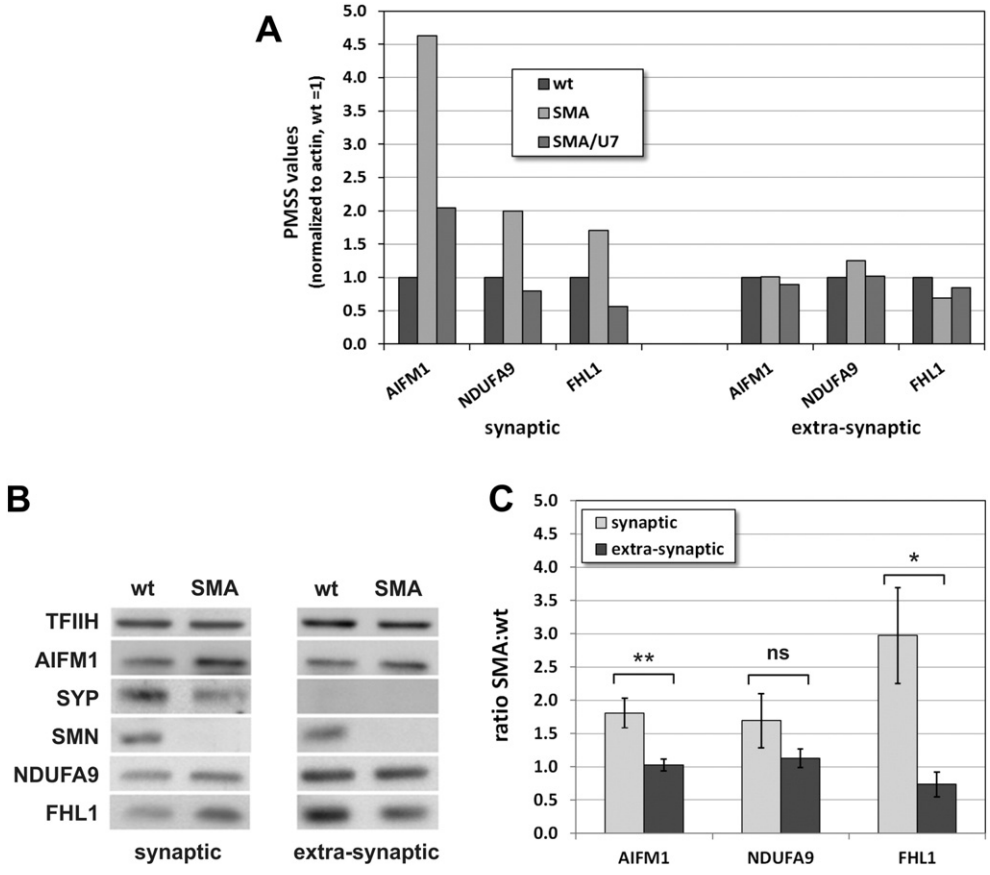

Fig. 5. Validation of mass spectrometry candidates. (A) Relative PMSS values from MS analysis. After normalization of the original values to that of actin in the same sample, the wt value has always been set as 1. The selected candidates are AIFM1, apoptosis inducing factor 1; NDUFA9, NADH dehydrogenase [ubiquinone] 1 alpha subcomplex subunit 9; FHL1, four and half lim domain 1. (B) Validation by Western blots. Proteins were extracted from the synaptic and extra-synaptic regions of the diaphragm muscle of three SMA disease and wt mice at PND3. Anti-TFIIH was used as a loading control, and synaptophysin was used to test for the enrichment of the synaptic regions. (C) Quantitative analysis of Western blot signals. The blots were performed in biological triplicates, and signal intensity (in arbitrary units) was quantified and normalized to TFIIH. The graph shows the ratios of the signals from SMA mice to those of wt mice for the synaptic and extra-synaptic regions. Statistical analysis revealed that AIFM1 and FHL1 were significantly up-regulated in the synaptic-specific regions of SMA mice ($P = 0.0098$ and 0.013, respectively, unpaired two-tailed Student T-test). In contrast, NDUFA9, although it had a higher level of expression in the SMA synapse-specific region, this was not statistically significant. Error bars represent standard deviations.

et al., 2007). However, as we have analysed GlyT2/gephyrin synapses, it appears that inhibitory inputs are normal in motoneurons from SMA mice, but that the stimulatory and inhibitory inputs are not properly balanced.

The second aspect of motoneuron cell bodies which we found to be altered is the shape of mitochondria (Supplementary Fig. S1). The rounding which we observed could be an early sign of an apoptotic process. Even though this change is more subtle than the ones occurring in the pre- and post-synaptic compartments of the diaphragm's NMJs (Voigt et al., 2010), it suggests that the metabolism of the motoneurons may be disturbed. In the future, this phenomenon may be studied by electron microscopy or by using functionally relevant IHC probes. However, it is interesting to note that changes in mitochondrial morphology have previously been shown to affect mitochondrial physiology and impact cellular viability (Rintoul and Reynolds, 2010; Su et al., 2010). Moreover, mitochondrial dysfunction appears to be a common feature of many neurodegenerative disorders like ALS (Mattiazzi et al., 2002), Alzheimer's disease (Mecocci et al., 1994) and Huntington's disease (Quintanilla and Johnson, 2009).

At the level of diaphragm NMJs, we have analysed the neurotransmitter vesicles and active zones of axon terminals. Active zones are the areas of neurotransmitter release in the presynaptic membrane. Our results indicate that both the synaptic vesicle density and the numbers and areas of active zones are reduced in SMA mice compared to wt littermates (Fig. 2). As these changes were significant for the whole diaphragm NMJ population, they must either be particularly strong in the severely affected NMJs as defined by EM, or they must also occur in morphologically less affected NMJs. In any case, these results are suggestive of a significant impairment in synaptic transmission. This is also supported by recent studies in other mouse SMA models. In particular, Benito et al. observed a similar decrease in synaptic vesicle and active zone clustering which was accompanied by a reduction of the readily releasable and recycling pool of synaptic vesicles in the transversus abdominis muscle of the Δ7 SMA mice (Torres-Benito et al., 2011). Other studies revealed an abnormal synaptic transmission (Kong et al., 2009) and an alteration of intracellular calcium homeostasis (Ruiz et al., 2010) in NMJs of Δ7 SMA mice. A significant decrease in calcium-dependent neurotransmitter release was also later reported for the A2G mouse SMA model (Ruiz and Tabares, 2014).

The importance of non-neuronal cells for the pathogenesis of SMA has become increasingly recognized over the past few years (Hamilton and Gillingwater, 2013). Defects in myelinating Schwann cells (Hunter et al., 2013; Murray et al., 2010a) as well as perineurial Schwann cells and perineurial fibroblasts (Voigt et al., 2010) have been described in SMA mouse models. These changes might affect the survival or functions of the axon, its terminal branches or even the motoneuron as a whole. Another type of glial cell that is more specifically relevant for the maintenance of a functional NMJ is the terminal or perisynaptic Schwann cell (PSC) (Auld and Robitaille, 2003; Feng and Ko, 2007). Our ultrastructural analyses of NMJs in the severe SMA model were the first to demonstrate morphological changes associated with these cells (Voigt et al., 2010, 2014). The vacuole-like inclusions in the PSC cytoplasm observed in these studies in fact appeared to precede other morphologic changes such as the swelling of mitochondria in the axon terminals and muscle fibres. Here, we have analysed the staining of PSCs with an antibody against the Schwann cell marker S100 (Fig. 3). This was significantly reduced for the partly innervated NMJs in SMA mice, and some NMJs even showed no detectable S100 staining at all, which contrasts with our EM analyses that revealed cells covering the axon terminals, even in the most strongly affected NMJs (Voigt et al., 2010, 2014). This indicates that the vacuolized cells that can be seen to cover the affected NMJs by EM must either be PSCs that have lost their Schwann cell identity or completely different cells that have replaced the PSCs. The first of these possibilities appears more likely and would imply that the PSCs dedifferentiate or transdifferentiate into another cell type in SMA-affected muscles or that the loss of S100 staining is an early symptom of an apoptotic process.

Whichever is the case, the changes occurring in PSCs are highly relevant for the maintenance and function of the corresponding NMJs. PSCs are important components of the NMJ, capable of modulating synaptic activity and contributing to synapse remodelling (Feng and Ko, 2007). They also promote synaptogenesis during development (Feng and Ko, 2008) or in the renervation after a nerve injury (Reynolds and Woolf, 1992; Son et al., 1996). A complex network of signalling interactions between PSCs, axon terminals and muscle fibres (which is still not fully understood) ensures that all three cellular components of a NMJ can fulfil their different roles (Feng and Ko, 2007). It would be interesting to know whether and how these signalling interactions are altered in SMA. This might also reveal new potential targets for a treatment of SMA.

Since our initial observation that PSCs are affected in severe SMA mice (Voigt et al., 2010), other studies have found a reduction of PSCs associated with the NMJs of the sternomastoid and soleus muscle of SMNΔ7 mice at PND13 (Lee et al., 2011) and the LAL-r muscle at PND21 of $Smn^{2B/-}$ mice (Murray et al., 2013). Moreover, PSCs seem to play a role in other neuromuscular disorders. An earlier study showed that a mouse mutant defective in the *SCN8A* gene that encodes the Nav1.6 voltage-gated sodium channel has a motor endplate disease phenotype and shows a reduced S100 staining at NMJs (Musarella et al., 2006). In humans, mutations of the *SCN8A* gene have been found in patients with cognitive disorders, sometimes associated with ataxia (Trudeau et al., 2006). More important for human motoneuron diseases, a dysfunction of PSCs has recently been implicated in a slowly progressive model of Amyotropic Lateral Sclerosis (ALS) (Arbour et al., 2015).

Differential proteomic studies provide a rapid and powerful insight into gene expression changes. However, for diseases of the neuromuscular system, it is important to use enriched preparations of the relevant structures. With respect to SMA, Wishart and coworkers have recently analysed the proteomic composition of biochemically isolated synaptosome preparations from the hippocampus of newborn SMA mice (Wishart et al., 2014) and from Schwann cells isolated from peripheral nerves (Aghamaleky Sarvestany et al., 2014). This led to the identification of the ubiquitin-like modifier activating enzyme 1 (UBA1) as a widely perturbed gene product that controls β-catenin signalling and nerve myelination. However, in muscle tissue, the NMJs are usually dispersed and difficult if not impossible to isolate. Consequently, only one study has so far looked at the proteomic composition of an entire muscle of SMA mice (Mutsaers et al., 2011).

In our case, we have exploited the fact that the diaphragm is very thin and that the NMJs are aligned in a band along the muscle to perform a proteomic study of synapse-specific and extra-synaptic regions. The achieved enrichment is considerable, considering the Western blot data for SYP and the proteomics result for the related protein SYPL2. The method can probably still be improved and scaled up to allow for an even deeper exploration of the NMJ proteome. Thus, a systems biology study of the diaphragm could be interesting well beyond its relevance for SMA.

An important outcome of our analysis is that over 40% of the differentially expressed proteins in the synaptic regions of SMA mouse diaphragms have catalytic activity and play an important role in the mitochondrial respiratory chain. This finding is interesting as we have previously observed by electron microscopy a massive mitochondrial swelling and degeneration in the axon terminals and sub-synaptic muscle fibre areas of the most severely affected NMJs (Voigt et al., 2010). However, we have to state that mitochondrial components are also highly represented in the extra-synaptic proteins and in the group of synaptic proteins that show little or no changes in expression. This most likely reflects the fact that muscle is generally rich in mitochondria. Nevertheless, the proportion of mitochondrial components is particularly high in the differentially expressed proteins from the synaptic

fractions and among these predominantly in the up-regulated group. This trend towards up-regulation of these components is somewhat surprising. Based on the massive degeneration of mitochondria visualized by EM, we would have expected a reduction rather than an up-regulation of mitochondrial proteins. Indeed, a recent study identified reductions in a number of mitochondrial markers in muscle tissues from human SMA type I and type II patients (Ripolone et al., 2015). The difference could be that these tissues came from patients at an advanced stage of the disease whereas the mouse diaphragm samples which we analysed only began to develop disease symptoms. The up-regulation observed in our proteomic approach might represent an adaptive response to disease-associated stress. In agreement with this idea, a compensatory increase in mitochondrial activity has recently been described in a cell culture SMN depletion model (Acsadi et al., 2009). At a certain point, however, the stressor thresholds might increase to levels which negatively impact mitochondrial integrity, eventually leading to their degeneration.

Two of the changes in protein abundance that we could validate concern regulatory proteins (FHL1 and AIFM1). Both were upregulated in the NMJ-enriched samples of SMA mice compared to wt littermates (Fig. 4), but showed no changes in the extrasynaptic region of the diaphragm (Fig. 4) or in cervical spinal cord (Supplementary Fig. S2). For technical reasons, we have not yet been able to identify in which cells of the synapse-enriched area the expression of these proteins is changed. However, based on their known biology (see next paragraphs), the increase of FHL1 is likely to occur mostly in muscle fibres and that of AIFM1 predominantly in motoneurons.

The four and a half lim domain protein 1 (FHL1) is enriched in skeletal muscle where it is an important regulator of muscle mass, and several lines of evidence suggest a correlation between FHL1 and muscular hypertrophy (Cowling et al., 2008; Loughna et al., 2000). In this sense, its up-regulation could be part of a compensatory mechanism of muscle remodelling to cope with the loss of functionality caused by the disease. Interestingly, the presence of atrophic and hypertrophic fibres has been reported in SMA patients (Buchthal and Olsen, 1970; Emery, 1971; Millino et al., 2009). Moreover, FHL1 has recently been identified as a therapeutic target for Duchenne Muscular Dystrophy (D'Arcy et al., 2014) and its loss induces a pronounced skeletal myopathy (Domenighetti et al., 2014).

The other validated upregulated protein is apoptosis inducing factor 1 (AIFM1), a mitochondrial inner membrane flavoprotein which has a role in controlling apoptosis in a caspase-independent pathway (Joza et al., 2001; Kroemer et al., 2007). In vertebrates, most of the cell death occurs via a pathway that involves mitochondrial membrane permeabilization. Upon the initiation of apoptosis, AIFM1 gets translocated to the nucleus, where it causes chromatin condensation and fragmentation of DNA. AIFM1 mutations have been associated with neurological and neurodegenerative conditions such as an X-linked Charcot–Marie–Tooth disease (CMTX4) with axonal sensorimotor neuropathy (Rinaldi et al., 2012), Alzheimer's disease (Lee et al., 2012) or a severe infantile motor neuron disease (Diodato et al., 2015). This highlights the importance of normal AIFM1 expression in motoneurons. Thus, the up-regulation of AIFM1 in the synaptic regions of the diaphragm of SMA mice that we have observed might be a response from burdened motoneurons.

An important question is how all the events highlighted in this study are related to each other and which cells are most important for triggering the disease. A motor unit is composed of a motoneuron, the muscle fibre(s) it innervates and the PSCs sitting at its NMJs. Additionally, the motoneuron receives inputs from afferent dorsal root neurons as well as from other neurons in the spinal cord and in higher brain centres. The data presented here indicate that an early reduction in VGLUT1 inputs might be an important contributor to motoneuron damage. Similarly, at the periphery, the early changes affecting PSCs may be a cause of the degenerative events that impair NMJ function. Whether the PSCs degenerate independently because of intrinsic low SMN levels or whether they react to subtle initial changes in the motoneurons is an open question. Similarly, the neurons that provide excitatory inputs to the alpha-motoneurons might be primary sensors of low SMN levels or, since most of them are proprioceptive neurons, they could be part of a feedback loop that aggravates the motoneuron's functionality. It is also not clear which events, those occurring in MN cell bodies or those occurring at the NMJs are occurring first and if there is a cause–effect relationship between them. Either the events in NMJs (axon terminals and PSCs) are the primary effect of the disease, and the reduction in excitatory inputs on MNs is due to some feed-back mechanism, or the central defect in excitatory inputs ultimately induces the peripheral defects. To answer these questions conclusively will be very difficult, even if the events are studied at earlier time points. Importantly, our data indicate that, at the stage that we have analysed, degenerative events have begun to affect the motor units both centrally and in the periphery.

Conflict of interest statement

The authors declare to have no conflicts of interest.

Acknowledgements

This work was supported by the Swiss National Science Foundation (grants 31003A-120064, 31003A_135644 and 31003A_153199), AFM (Association Française contre les Myopathies), and the Kanton Bern. We thank Manfred Heller for mass spectrometry analyses and Marc Ruepp for SMN antibody preparation.

A.N. performed all experiments. J.T. was responsible for mouse breeding and genotyping and participated in the preparation of samples. S.S. provided helpful suggestions, equipment and reagents throughout the study. A.N. and D.S. conceived the study and wrote the manuscript. D.S. secured financial support.

Appendix A. Supplementary data

Supplementary data to this article can be found online at http://dx.doi.org/10.1016/j.mcn.2015.11.007.

References

Acsadi, G., Lee, I., Li, X., Khaidakov, M., Pecinova, A., Parker, G.C., Hüttemann, M., 2009. Mitochondrial dysfunction in a neural cell model of spinal muscular atrophy. J. Neurosci. Res. 87, 2748–2756.

Aghamaleky Sarvestany, A., Hunter, G., Tavendale, A., Lamont, D.J., Llavero Hurtado, M., Graham, L.C., Wishart, T.M., Gillingwater, T.H., 2014. Label-free quantitative proteomic profiling identifies disruption of ubiquitin homeostasis as a key driver of Schwann cell defects in spinal muscular atrophy. J. Proteome Res. 13, 4546–4557.

Alías, L., Bernal, S., Fuentes-Prior, P., Barceló, M.J., Also, E., Martínez-Hernández, R., Rodríguez-Alvarez, F.J., Martín, Y., Aller, E., Grau, E., 2009. Mutation update of spinal muscular atrophy in Spain: molecular characterization of 745 unrelated patients and identification of four novel mutations in the SMN1 gene. Hum. Genet. 125, 29–39.

Anagnostou, E., Miller, S.P., Guiot, M.-C., Karpati, G., Simard, L., Dilenge, M.-E., Shevell, M.I., 2005. Type I spinal muscular atrophy can mimic sensory-motor axonal neuropathy. J. Child Neurol. 20, 147–150.

Arbour, D., Tremblay, E., Martineau, É., Julien, J.-P., Robitaille, R., 2015. Early and persistent abnormal decoding by glial cells at the neuromuscular junction in an ALS model. J. Neurosci. 35, 688–706.

Auld, D., Robitaille, R., 2003. Perisynaptic Schwann cells at the neuromuscular junction: nerve-and activity-dependent contributions to synaptic efficacy, plasticity, and reinnervation. Neuroscientist 9, 144.

Baker, M.J., Tatsuta, T., Langer, T., 2011. Quality control of mitochondrial proteostasis. Cold Spring Harb. Perspect. Biol. 3, a007559.

Barbour, J.A., Turner, N., 2014. Mitochondrial stress signaling promotes cellular adaptations. Int. J. Cell Biol. 2014.

Ben-Ari, Y., Gaiarsa, J.-L., Tyzio, R., Khazipov, R., 2007. GABA: a pioneer transmitter that excites immature neurons and generates primitive oscillations. Physiol. Rev. 87, 1215–1284.

Buchthal, F., Olsen, P., 1970. Electromyography and muscle biopsy in infantile spinal muscular atrophy. Brain J. Neurol. 93, 15.

Burghes, A., 1997. When is a deletion not a deletion? When it is converted. Am. J. Hum. Genet. 61, 9.

Cartegni, L., Krainer, A.R., 2002. Disruption of an SF2/ASF-dependent exonic splicing enhancer in SMN2 causes spinal muscular atrophy in the absence of SMN1. Nat. Genet. 30, 377–384.
Cartegni, L., Hastings, M.L., Calarco, J.A., de Stanchina, E., Krainer, A.R., 2006. Determinants of exon 7 splicing in the spinal muscular atrophy genes, SMN1 and SMN2. Am. J. Hum. Genet. 78, 63–77.
Chang, Q., Martin, L.J., 2009. Glycinergic innervation of motoneurons is deficient in amyotrophic lateral sclerosis mice: a quantitative confocal analysis. Am. J. Pathol. 174, 574–585.
Cope, T.C., 2001. Motor Neurobiology of the Spinal Cord. CRC Press.
Cowling, B.S., McGrath, M.J., Nguyen, M.-A., Cottle, D.L., Kee, A.J., Brown, S., Schessl, J., Zou, Y., Joya, J., Bönnemann, C.G., Hardeman, E.C., Mitchell, C.A., 2008. Identification of FHL1 as a regulator of skeletal muscle mass: implications for human myopathy. J. Cell Biol. 183, 1033–1048.
Crawford, T.O., 2003. Spinal Muscular Atrophies. Neuromuscular Disorders of Infancy, Childhood, and Adolescence: A Clinician's Approach. Butterworth Heinemann, Philadelphia, PA, pp. 145–166.
Dachs, E., Hereu, M., Piedrafita, L., Casanovas, A., Calderó, J., Esquerda, J.E., 2011. Defective neuromuscular junction organization and postnatal myogenesis in mice with severe spinal muscular atrophy. J. Neuropathol. Exp. Neurol. 70, 444–461 (410.1097/NEN.1090b1013e31821cbd31828b).
D'Arcy, C.E., Feeney, S.J., McLean, C.A., Gehrig, S.M., Lynch, G.S., Smith, J.E., Cowling, B.S., Mitchell, C.A., McGrath, M.J., 2014. Identification of FHL1 as a therapeutic target for Duchenne muscular dystrophy. Hum. Mol. Genet. 23, 618–636.
Diodato, D., Tasca, G., Verrigni, D., D'Amico, A., Rizza, T., Tozzi, G., Martinelli, D., Verardo, M., Invernizzi, F., Nasca, A., Bellacchio, E., Ghezzi, D., Piemonte, F., Dionisi-Vici, C., Carrozzo, R., Bertini, E., 2015. A novel AIFM1 mutation expands the phenotype to an infantile motor neuron disease. Eur. J. Hum. Genet. http://dx.doi.org/10.1038/ejhg.2015.141 (Epub ahead of print).
Domenighetti, A.A., Chu, P.-H., Wu, T., Sheikh, F., Gokhin, D.S., Guo, L.T., Cui, Z., Peter, A.K., Christodoulou, D.C., Parfenov, M.G., Gorham, J.M., Li, D.Y., Banerjee, I., Lai, X., Witzmann, F.A., Seidman, C.E., Seidman, J.G., Gomes, A.V., Shelton, G.D., Lieber, R.L., Chen, J., 2014. Loss of FHL1 induces an age-dependent skeletal muscle myopathy associated with myofibrillar and intermyofibrillar disorganization in mice. Hum. Mol. Genet. 23, 209–225.
Emery, A., 1971. The nosology of the spinal muscular atrophies. J. Med. Genet. 8, 481.
Feng, Z., Ko, C.P., 2007. Neuronal glia interactions at the vertebrate neuromuscular junction. Curr. Opin. Pharmacol. 7, 316–324.
Feng, Z., Ko, C.-P., 2008. Schwann cells promote synaptogenesis at the neuromuscular junction via transforming growth factor-β1. J. Neurosci. 28, 9599–9609.
Frank, S., Gaume, B., Bergmann-Leitner, E.S., Leitner, W.W., Robert, E.G., Catez, F., Smith, C.L., Youle, R.J., 2001. The role of dynamin-related protein 1, a mediator of mitochondrial fission, in apoptosis. Dev. Cell 1, 515–525.
Hamilton, G., Gillingwater, T.H., 2013. Spinal muscular atrophy: going beyond the motor neuron. Trends Mol. Med. 19, 40–50.
Hunter, G., Sarvestany, A.A., Roche, S.L., Symes, R.C., Gillingwater, T.H., 2013. SMN-dependent intrinsic defects in Schwann cells in mouse models of spinal muscular atrophy. Hum. Mol. Genet. (ddt612).
Imlach, W.L., Beck, E.S., Choi, B.J., Lotti, F., Pellizzoni, L., McCabe, B.D., 2012. SMN is required for sensory-motor circuit function in *Drosophila*. Cell 151, 427–439.
Jablonka, S., Karle, K., Sandner, B., Andreassi, C., von Au, K., Sendtner, M., 2006. Distinct and overlapping alterations in motor and sensory neurons in a mouse model of spinal muscular atrophy. Hum. Mol. Genet. 15, 511–518.
Jiang, M., Schuster, J.E., Fu, R., Siddique, T., Heckman, C., 2009. Progressive changes in synaptic inputs to motoneurons in adult sacral spinal cord of a mouse model of amyotrophic lateral sclerosis. J. Neurosci. 29, 15031–15038.
Joza, N., Susin, S.A., Daugas, E., Stanford, W.L., Cho, S.K., Li, C.Y., Sasaki, T., Elia, A.J., Cheng, H.-Y.M., Ravagnan, L., 2001. Essential role of the mitochondrial apoptosis-inducing factor in programmed cell death. Nature 410, 549–554.
Kariya, S., Park, G.H., Maeno-Hikichi, Y., Leykekhman, O., Lutz, C., Arkovitz, M.S., Landmesser, L.T., Monani, U.R., 2008. Reduced SMN protein impairs maturation of the neuromuscular junctions in mouse models of spinal muscular atrophy. Hum. Mol. Genet. 17, 2552–2569.
Kashima, T., Manley, J.L., 2003. A negative element in SMN2 exon 7 inhibits splicing in spinal muscular atrophy. Nat. Genet. 34, 460–463.
Kong, L., Wang, X., Choe, D.W., Polley, M., Burnett, B.G., Bosch-Marcé, M., Griffin, J.W., Rich, M.M., Sumner, C.J., 2009. Impaired synaptic vesicle release and immaturity of neuromuscular junctions in spinal muscular atrophy mice. J. Neurosci. 29, 842–851.
Kroemer, G., Galluzzi, L., Brenner, C., 2007. Mitochondrial membrane permeabilization in cell death. Physiol. Rev. 87, 99–163.
Lee, Y.i., Mikesh, M., Smith, I., Rimer, M., Thompson, W., 2011. Muscles in a mouse model of spinal muscular atrophy show profound defects in neuromuscular development even in the absence of failure in neuromuscular transmission or loss of motor neurons. Dev. Biol. 356, 432–444.
Lee, J.-H., Cheon, Y.-H., Woo, R.-S., Song, D.-Y., Moon, C., Baik, T.-K., 2012. Evidence of early involvement of apoptosis inducing factor-induced neuronal death in Alzheimer brain. Anat. Cell Biol. 45, 26–37.
Lefebvre, S., Bürglen, L., Reboullet, S., Clermont, O., Burlet, P., Viollet, L., Benichou, B., Cruaud, C., Millasseau, P., Zeviani, M., 1995. Identification and characterization of a spinal muscular atrophy-determining gene. Cell 80, 155–165.
Ling, K.K., Lin, M.-Y., Zingg, B., Feng, Z., Ko, C.-P., 2010. Synaptic defects in the spinal and neuromuscular circuitry in a mouse model of spinal muscular atrophy. PLoS One 5, e15457.
Ling, K.K., Gibbs, R.M., Feng, Z., Ko, C.-P., 2012. Severe neuromuscular denervation of clinically relevant muscles in a mouse model of spinal muscular atrophy. Hum. Mol. Genet. 21, 185–195.
Lorson, C.L., Androphy, E.J., 2000. An exonic enhancer is required for inclusion of an essential exon in the SMA-determining gene SMN. Hum. Mol. Genet. 9, 259–265.
Lorson, C., Hahnen, E., Androphy, E., Wirth, B., 1999. A single nucleotide in the SMN gene regulates splicing and is responsible for spinal muscular atrophy. Proc. Natl. Acad. Sci. U. S. A. 96, 6307.
Loughna, P.T., Mason, P., Bayol, S., Brownson, C., 2000. The LIM-domain protein FHL1 (SLIM 1) exhibits functional regulation in skeletal muscle. Mol. Cell Biol. Res. Commun. 3, 136–140.
Mattiazzi, M., D'Aurelio, M., Gajewski, C.D., Martushova, K., Kiaei, M., Beal, M.F., Manfredi, G., 2002. Mutated human SOD1 causes dysfunction of oxidative phosphorylation in mitochondria of transgenic mice. J. Biol. Chem. 277, 29626–29633.
McGovern, V.L., Gavrilina, T.O., Beattie, C.E., Burghes, A.H.M., 2008. Embryonic motor axon development in the severe SMA mouse. Hum. Mol. Genet. 17, 2900–2909.
Mecocci, P., MacGarvey, U., Beal, M.F., 1994. Oxidative damage to mitochondrial DNA is increased in Alzheimer's disease. Ann. Neurol. 36, 747–751.
Mentis, G.Z., Blivis, D., Liu, W., Drobac, E., Crowder, M.E., Kong, L., Alvarez, F.J., Sumner, C.J., O'Donovan, M.J., 2011. Early functional impairment of sensory-motor connectivity in a mouse model of spinal muscular atrophy. Neuron 69, 453–467.
Meyer, K., Marquis, J., Trüb, J., Nlend Nlend, R., Verp, S., Ruepp, M., Imboden, H., Barde, I., Trono, D., Schümperli, D., 2009. Rescue of a severe mouse model for spinal muscular atrophy by U7 snRNA-mediated splicing modulation. Hum. Mol. Genet. 18, 546.
Michaud, M., Arnoux, T., Bielli, S., Durand, E., Rotrou, Y., Jablonka, S., Robert, F., Giraudon-Paoli, M., Riessland, M., Mattei, M.G., Andriambeloson, E., Wirth, B., Sendtner, M., Gallego, J., Pruss, R.M., Bordet, T., 2010. Neuromuscular defects and breathing disorders in a new mouse model of spinal muscular atrophy. Neurobiol. Dis. 38, 125–135.
Millino, C., Fanin, M., Vettori, A., Laveder, P., Mostacciuolo, M.L., Angelini, C., Lanfranchi, G., 2009. Different atrophy–hypertrophy transcription pathways in muscles affected by severe and mild spinal muscular atrophy. BMC Med. 7, 14.
Monani, U.R., Lorson, C.L., Parsons, D.W., Prior, T.W., Androphy, E.J., Burghes, A.H., McPherson, J.D., 1999. A single nucleotide difference that alters splicing patterns distinguishes the SMA gene SMN1 from the copy gene SMN2. Hum. Mol. Genet. 8, 1177–1183.
Monani, U.R., Sendtner, M., Coovert, D.D., Parsons, D.W., Andreassi, C., Le, T.T., Jablonka, S., Schrank, B., Rossol, W., Prior, T.W., 2000. The human centromeric survival motor neuron gene (SMN2) rescues embryonic lethality in Smn −/− mice and results in a mouse with spinal muscular atrophy. Hum. Mol. Genet. 9, 333–339.
Murray, L.M., Comley, L.H., Thomson, D., Parkinson, N., Talbot, K., Gillingwater, T.H., 2008. Selective vulnerability of motor neurons and dissociation of pre- and post-synaptic pathology at the neuromuscular junction in mouse models of spinal muscular atrophy. Hum. Mol. Genet. 17, 949–962.
Murray, L.M., Lee, S., Bäumer, D., Parson, S.H., Talbot, K., Gillingwater, T.H., 2010a. Pre-symptomatic development of lower motor neuron connectivity in a mouse model of severe spinal muscular atrophy. Hum. Mol. Genet. 19, 420.
Murray, L.M., Talbot, K., Gillingwater, T.H., 2010b. Review: neuromuscular synaptic vulnerability in motor neurone disease: amyotrophic lateral sclerosis and spinal muscular atrophy. Neuropathol. Appl. Neurobiol. 36, 133–156.
Murray, L.M., Beauvais, A., Bhanot, K., Kothary, R., 2013. Defects in neuromuscular junction remodelling in the *Smn*$^{2B/-}$ mouse model of spinal muscular atrophy. Neurobiol. Dis. 49, 57–67.
Musarella, M., Alcaraz, G., Caillol, G., Boudier, J.-L., Couraud, F., Autillo-Touati, A., 2006. Expression of Nav1.6 sodium channels by Schwann cells at neuromuscular junctions: role in the motor endplate disease phenotype. Glia 53, 13–23.
Mutsaers, C.A., Wishart, T.M., Lamont, D.J., Riessland, M., Schreml, J., Comley, L.H., Murray, L.M., Parson, S.H., Lochmuller, H., Wirth, B., Talbot, K., Gillingwater, T.H., 2011. Reversible molecular pathology of skeletal muscle in spinal muscular atrophy. Hum. Mol. Genet.
Park, G.-H., Maeno-Hikichi, Y., Awano, T., Landmesser, L.T., Monani, U.R., 2010. Reduced survival of motor neuron (SMN) protein in motor neuronal progenitors functions cell autonomously to cause spinal muscular atrophy in model mice expressing the human centromeric (SMN2) gene. J. Neurosci. 30, 12005–12019.
Quintanilla, R.A., Johnson, G.V.W., 2009. Role of mitochondrial dysfunction in the pathogenesis of Huntington's disease. Brain Res. Bull. 80, 242–247.
Reynolds, M.L., Woolf, C.J., 1992. Terminal Schwann cells elaborate extensive processes following denervation of the motor endplate. J. Neurocytol. 21, 50–66.
Rinaldi, C., Grunseich, C., Sevrioukova, Irina F., Schindler, A., Horkayne-Szakaly, I., Lamperti, C., Landouré, G., Kennerson, Marina L., Burnett, Barrington G., Bönnemann, C., Biesecker, Leslie G., Ghezzi, D., Zeviani, M., Fischbeck, Kenneth H., 2012. Cowchock Syndrome Is Associated with a Mutation in Apoptosis-Inducing Factor. Am. J. Hum. Genet 91, 1095–1102.
Rintoul, G.L., Reynolds, I.J., 2010. Mitochondrial trafficking and morphology in neuronal injury. Biochim. Biophys. Acta (BBA) - Mol. Basis Dis. 1802, 143–150.
Ripolone, M., Ronchi, D., Violano, R., Vallejo, D., Fagiolari, G., Barca, E., Lucchini, V., Colombo, I., Villa, L., Berardinelli, A., Balottin, U., Morandi, L., Mora, M., Bordoni, A., Fortunato, F., Corti, S., Parisi, D., Toscano, A., Sciacco, M., DiMauro, S., Comi, G.P., Moggio, M., 2015. Impaired muscle mitochondrial biogenesis and myogenesis in spinal muscular atrophy. JAMA Neurol. 72, 666–675.
Rodrigues, N., Owen, N., Talbot, K., Ignatius, J., Dubowitz, V., Davies, K., 1995. Deletions in the survival motor neuron gene on 5q13 in autosomal recessive spinal muscular atrophy. Hum. Mol. Genet. 4, 631–634.
Rudnik-Schöneborn, S., Goebel, H., Schlote, W., Molaian, S., Omran, H., Ketelsen, U., Korinthenberg, R., Wenzel, D., Lauffer, H., Kreiss-Nachtsheim, M., 2003. Classical infantile spinal muscular atrophy with SMN deficiency causes sensory neuronopathy. Neurology 60, 983–987.
Ruiz, R., Tabares, L., 2014. Neurotransmitter release in motor nerve terminals of a mouse model of mild spinal muscular atrophy. J. Anat. 224, 74–84.

Ruiz, R., Casañas, J.J., Torres-Benito, L., Cano, R., Tabares, L., 2010. Altered intracellular Ca^{2+} homeostasis in nerve terminals of severe spinal muscular atrophy mice. J. Neurosci. 30, 849–857.

Schmutz, J., Martin, J., Terry, A., Couronne, O., Grimwood, J., Lowry, S., Gordon, L.A., Scott, D., Xie, G., Huang, W., 2004. The DNA sequence and comparative analysis of human chromosome 5. Nature 431, 268–274.

Schütz, B., 2005. Imbalanced excitatory to inhibitory synaptic input precedes motor neuron degeneration in an animal model of amyotrophic lateral sclerosis. Neurobiol. Dis. 20, 131–140.

Son, Y.-J., Trachtenberg, J.T., Thompson, W.J., 1996. Schwann cells induce and guide sprouting and reinnervation of neuromuscular junctions. Trends Neurosci. 19, 280–285.

Su, B., Wang, X., Zheng, L., Perry, G., Smith, M.A., Zhu, X., 2010. Abnormal mitochondrial dynamics and neurodegenerative diseases. Biochim. Biophys. Acta (BBA) - Mol. Basis Dis. 1802, 135–142.

Thomson, S.R., Nahon, J.E., Mutsaers, C.A., Thomson, D., Hamilton, G., Parson, S.H., Gillingwater, T.H., 2012. Morphological characteristics of motor neurons do not determine their relative susceptibility to degeneration in a mouse model of severe spinal muscular atrophy. PLoS One 7, e52605.

Torres-Benito, L., Neher, M.F., Cano, R., Ruiz, R., Tabares, L., 2011. SMN requirement for synaptic vesicle, active zone and microtubule postnatal organization in motor nerve terminals. PLoS One 6, e26164.

Trudeau, M.M., Dalton, J.C., Day, J.W., Ranum, L.P., Meisler, M.H., 2006. Heterozygosity for a protein truncation mutation of sodium channel SCN8A in a patient with cerebellar atrophy, ataxia, and mental retardation. J. Med. Genet. 43, 527–530.

Voigt, T., Meyer, K., Baum, O., Schümperli, D., 2010. Ultrastructural changes in diaphragm neuromuscular junctions in a severe mouse model for Spinal Muscular Atrophy and their prevention by bifunctional U7 snRNA correcting SMN2 splicing. Neuromuscul. Disord. 20, 744–752.

Voigt, T., Neve, A., Schümperli, D., 2014. The craniosacral progression of muscle development influences the emergence of neuromuscular junction alterations in a severe murine model for spinal muscular atrophy. Neuropathol. Appl. Neurobiol. 40, 416–434.

Wishart, T.M., Mutsaers, C.A., Riessland, M., Reimer, M.M., Hunter, G., Hannam, M.L., Eaton, S.L., Fuller, H.R., Roche, S.L., Somers, E., Morse, R., Young, P.J., Lamont, D.J., Hammerschmidt, M., Joshi, A., Hohenstein, P., Morris, G.E., Parson, S.H., Skehel, P.A., Becker, T., Robinson, I.M., Becker, C.G., Wirth, B., Gillingwater, T.H., 2014. Dysregulation of ubiquitin homeostasis and beta-catenin signaling promote spinal muscular atrophy. J. Clin. Invest. 124, 1821–1834.